Numerical and experimental study of first passage time of a steel strip subjected to forced and parametric excitations

E. Delhez [1], **H. Vanvinckenroye** [2], **J.-C. Golinval** [1], **V. Denoël** [2]
[1] University of Liège, Department of Aerospace and Mechanical Engineering,
Quartier Polytech 1, Allée de la Découverte, 9, 4000 Liège, Belgium.

[2] University of Liège, Department of Urban and Environmental Engineering.

Abstract
The first passage time refers to the time required for a dynamical system to reach a target energy level for the first time, departing from a known initial state. Analytical studies of the first passage time of a linear Mathieu oscillator under stochastic forced and parametric excitations defined as δ-correlated Brownian noises identified three behavioral regimes for the first passage time. The current work describes the design and use of an experimental set-up in order to validate the existence of the regimes. This paper successively describes the design and the finite element modeling of the set-up consisting in a pre-stressed steel strip, the reduction of the system to a single-degree-of-freedom system to match the framework of the theory, numerical studies on the influence of the frequency bands of the excitations on the first passage time and the experimental tests. Qualitatively, two of the three regimes are successfully observed in the experiment. Quantitatively, a good match is observed between the experimental and model results.

1 Introduction

The dynamics of many systems can be described by the Mathieu equation

$$z'' + 2\xi z' + [1 + u(\tau)]\, z = w(\tau), \tag{1}$$

where z is the dependent state variable, τ is a dimensionless time and ξ is the damping coefficient of the system. The right-hand side $w(\tau)$ represents an external force applied to the system and will be referred to as the forced excitation in the following. By contrast, the function $u(\tau)$ is a parametric excitation, as it induces variation in time of the stiffness of the oscillator. This equation can for instance model the oscillations of a pendulum in the gravity field when its support is subjected to a vertical motion, the parametric vibrations of cables subjected to axial oscillations at one extremity or the rotative equilibrium of a crane in a turbulent wind [4, 5, 8].

Equation (1) has been widely studied in the deterministic case, *i.e.* when the forced and parametric excitations have known deterministic analytical expressions, in particular in the harmonic case, with the aim of characterizing its steady-state solution and its stability [1, 6]. However, in most realistic applications, the system is slightly damped and the forced and parametric excitations are stochastic processes, so that the system spends most of its time in a stochastic transient regime. In the stochastic context, the classical stability theories are no longer relevant and the theory of first passage time has been developed as an efficient alternative. It consists in determining the statistics of the first passage time, defined as the time required for a stochastic process to leave a domain for the first time when starting from a given initial state inside the domain.

Closed-form expressions of the first and second order moments of the first passage time have been derived when both the forced and parametric excitations w and u are δ-correlated Brownian noises [9, 10]. These analytical developments, based on a multiple-scale approach, have highlighted the influence of some dimensionless groups impacting the dynamics and the existence of three different behavioral regimes, namely the additive, the incubation and the multiplicative regimes.

The aim of this paper is to design an experiment with an intrinsically multi-degree-of-freedom system to relate the equivalent linear Mathieu equation to the physical parameters of the system and to provide new experimental evidence of the existence of the three regimes identified in [9].

This paper starts with the description of the experimental set-up. Then, a finite element model of the structure is built and experimental modal analysis techniques are used to update this model. The multi-degree-of-freedom governing equations are then reduced to a set of decoupled single-degree-of-freedom equations to fit in the framework defined by the theory. The conditions under which an efficient use of the reduced model can be done are determined. They naturally lead to a numerical study of the first passage time of systems subjected to narrow-band excitations for which analytical results are not yet available. Eventually, first passage time maps are built experimentally and compared with the predicted results.

2 Experimental set-up description

The experimental part of the work is conducted in the "LTAS - Vibrations et Identification des Structures" (LTAS-VIS) laboratory unit of the Department of Aerospace and Mechanical engineering at the University of Liège. The experimental set-up consists in a vertical strip pre-stressed by a mass $m = 1.816$ kg. A schematic representation of the set-up is given in Fig. 1. The strip is characterized by a length $\ell = 0.501$ m, a width $w = 25$ mm and a thickness $t = 0.4$ mm. The structure is made of carbon steel (Young's modulus $E = 206$ GPa and density $\rho = 7\,767$ kg/m^3). The strip is clamped at its top end while a lateral guide constrains the bottom end of the strip to move only in the vertical direction.

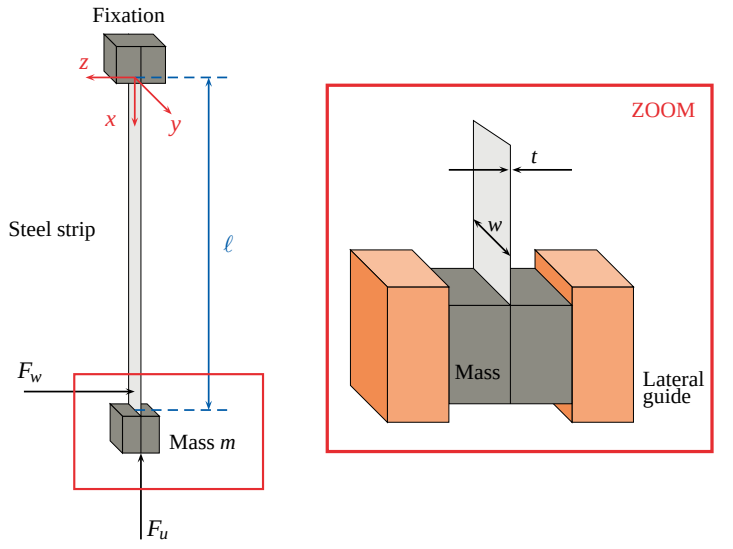

Figure 1: Schematic view of the designed experimental set-up.

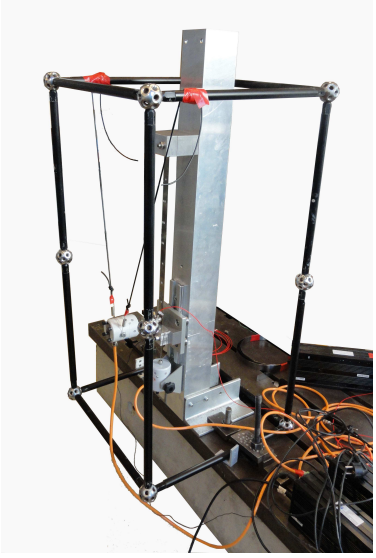

Figure 2: Experimental set-up.

The forced and parametric excitations F_w and F_u are applied by means of two electrodynamic vibration exciters. The first shaker is mounted horizontally and is used to excite the strip out of its plane close to its bottom fixation. This force constitutes the forced excitation of Mathieu equation (1). The second shaker is mounted vertically at the bottom of the structure, below the mass. This force modifies the pre-stress of the strip and therefore induces variation in time of the strip stiffness, giving rise to the parametric excitation of Mathieu equation. A picture of the physical prototype of the structure with the two shakers is given in Fig. 2.

Besides the two shakers, the structure is also instrumented with two impedance heads located at the two points where the shakers act and used to measure the force and the acceleration at these points. A Polytec MSA-400 OFV-552 laser transducer is used to measure the response of the structure in term of velocity at a single point. Data acquisition and signal processing are carried out using the LMS Test.Lab software and the LMS SCADAS Lab acquisition system [11].

3 Numerical modeling

In order to build an accurate numerical model of the physical set-up, both theoretical and experimental modal analyses are followed. The modal properties identified with these two approaches are then compared and the experimental results are used to update the finite element model. As a first step, a model of the non-instrumented structure (without the shakers) is built. Then, the influence of the shakers on the dynamics of the structure is modeled.

3.1 Non-instrumented structure

On the one hand, the steel strip is modeled in MATLAB using Bernoulli beam elements. The pre-stress is taken into account by the means of a geometrical stiffness matrix added to the usual linear stiffness matrix [3]. This numerical model is used to obtain a first estimate of the six lower natural frequencies and corresponding mode shapes of the strip.

On the other hand, experimental modal analysis is carried out on the real non-instrumented structure. The structure is excited close to its bottom fixation with an instrumented impact hammer and the response is successively measured at 8 other points equally spaced along the whole strip. The "Least Square Complex Exponential" (LSCE) and "Least Square Frequency Domain" (LSFD) methods are used to identify the modal properties of the structure [2].

The two sets of modal parameters obtained with the theoretical and experimental modal analyses are then compared. The natural frequencies obtained with the numerical model systematically overestimate the corresponding natural frequencies identified with the experimental modal analysis by 3-4%, which leaves room for improvement. The model is more rigid than the real structure. This can be ascribed to the modeling of the supports as perfect clampings. The finite element model is therefore corrected by introducing a stiffness in rotation about the y-axis (Fig. 1) at both ends of the strip. To simplify the analysis, the stiffness coefficient is assumed to be the same on both sides. The rigidity of the clamping is determined in such a way that it minimizes the difference (in a least-square sense) between the natural frequencies obtained with the numerical and experimental modal analyses. An optimum value of $k = 3.83$ Nm/rad is found.

This modification of the finite element model allows to decrease the relative errors on the natural frequencies below 0.2%. The Modal Assurance Criterion (MAC) [2] is used to quantify the correlation between the two sets of modes as represented in Fig. 3.

3.2 Instrumented structure

While the above derived model provides an accurate description of the dynamics of the strip itself, the shakers mounted on it have a non-negligible influence on the dynamics. Their influence has to be taken into account.

Experimental modal analysis is carried out by exciting the structure with the horizontal shaker located near the bottom fixation. The vertical shaker does not excite the structure but is mounted on it in such a way that its interaction with the structure is taken into account. The identification of the modal parameters of the structure is performed with the "Stochastic Subspace Identification" (SSI) method [7].

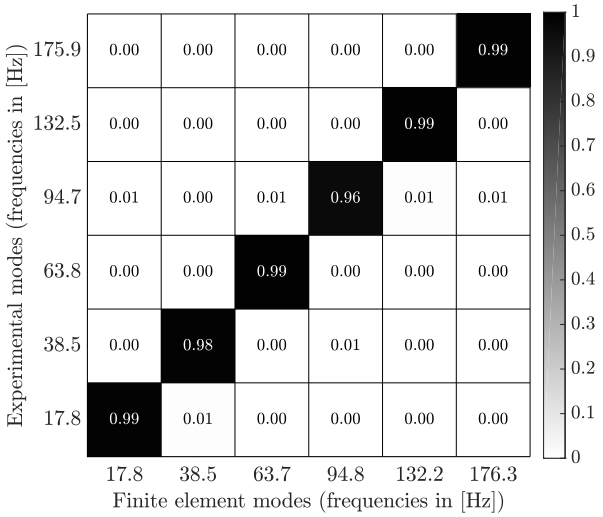

Figure 3: MAC matrix (non-instrumented structure).

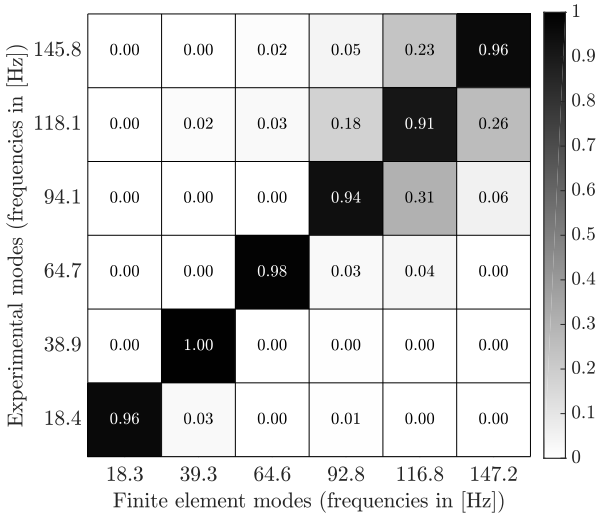

Figure 4: MAC matrix (instrumented structure).

The natural frequencies identified appear to differ by up to 20% from the natural frequencies computed with the original finite element model. The interaction of the shakers with the structure has therefore to be taken into account to get a reliable model.

The horizontal shaker, the stinger and the impedance head glued to the strip (Fig. 5) are modeled by a spring-mass system as shown in Fig. 6. The influence of the impedance head is modeled by adding a concentrated mass equal to the mass of the impedance head $m_{\text{head}} = 3 \cdot 10^{-2}$ kg where the horizontal shaker acts. The aluminum stinger connecting the shaker to the strip is modeled by a spring of stiffness $k_{\text{stinger}} = 4.5 \cdot 10^{6}$ N/m. The shaker itself is modeled by two masses connected by a spring. The mass $m_{\text{shaker}} = 1.7$ kg represents the main body of the shaker and the mass $m_{\text{moving}} = 1.5 \cdot 10^{-2}$ kg corresponds to the small moving mass. The spring of stiffness $k_{\text{suspension}} = 4 \cdot 10^{3}$ N/m represents the moving mass suspension. This modification of the finite element model reduces the relative errors on the natural frequencies below 5%.

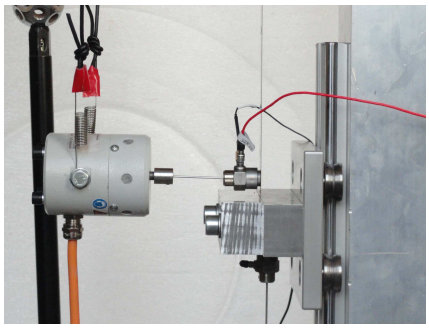

Figure 5: Horizontal shaker picture.

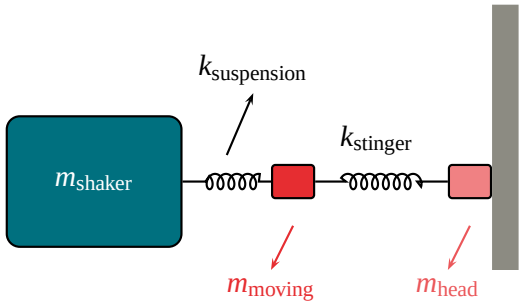

Figure 6: Horizontal shaker modeling.

The impedance head glued to the strip where the horizontal shaker acts prevents the strip from exhibiting significant curvature near the clamping. To reduce the errors, the stiffness of the finite elements in contact with the impedance head is artificially increased by 2%. This increased stiffness is adjusted to minimize the errors on the first six bending natural frequencies of the structure in a least square sense.

As a result of these two new modifications of the numerical finite element model of the structure, the relative errors on the natural frequencies are less than 1.2%. The corresponding MAC matrix is represented in Fig. 4 and shows a good correlation between the mode shapes and the corresponding frequencies. It is checked that the modes identified experimentally are real. A damping matrix that guarantees diagonal modal damping is built from the identified damping ratios using the assumption of proportional damping as proposed in [3].

4 From multiple-degree-of-freedom to single-degree-of-freedom equations of motion

The studied structure subjected to an external excitation $\mathbf{f}(t)$ is governed by the general equation of motion

$$\mathbf{M}\ddot{\mathbf{x}}(t) + \mathbf{C}\dot{\mathbf{x}}(t) + \mathbf{K}(t)\mathbf{x}(t) = \mathbf{f}(t), \tag{2}$$

where $\mathbf{x}$ is the vector of generalized coordinates, $\mathbf{M}$ the mass matrix, $\mathbf{C}$ the damping matrix and $\mathbf{K}(t)$ the time-varying stiffness matrix. The stiffness matrix can be decomposed into its constant and time-varying parts $\mathbf{K}(t) = \mathbf{K}_0 + \mathbf{K}_{\text{prestress}}(t)$, where $\mathbf{K}_0$ is the constant stiffness matrix and $\mathbf{K}_{\text{prestress}}(t)$ characterizes the time modulation of the stiffness induced by the zero mean parametric excitation $F_u(t)$. The multi-degree-of-freedom structure is therefore governed by a multi-dimensional version of the Mathieu equation.

The analytical results related to first passage time developed in [9] apply to single-degree-of-freedom Mathieu oscillators subjected to broadband forced and parametric excitations. In order to fit in the particular framework of the analytic model, several adaptations are required. This section focuses on the single-degree-of-freedom system model assumption. The multi-degree-of-freedom governing equations are reduced to a set of uncoupled single-degree-of-freedom Mathieu equations. The conditions under which a profitable use of this model reduction can be done are then identified.

4.1 Model reduction

The response of the structure $\mathbf{x}(t)$ can be written in the modal basis as $\mathbf{x}(t) = \mathbf{\Phi}\mathbf{q}(t)$, where $\mathbf{\Phi}$ is the modal matrix and $\mathbf{q}(t)$ is the vector of modal coordinates. Pre-multiplying the dynamical equation (2) by $\mathbf{\Phi}^{\mathrm{T}}$ and defining modal matrices and vectors as the projections of the physical structural matrices and vectors on the modal basis, the equation governing the dynamics of the modal coordinates can be written as

$$\mathbf{M}^*\ddot{\mathbf{q}}(t) + \mathbf{C}^*\dot{\mathbf{q}}(t) + [\mathbf{K}^* + F_u(t)\mathbf{K}^*_{\text{prestress,1}}]\mathbf{q}(t) = \mathbf{f}^*(t), \tag{3}$$

where $\mathbf{K}^*_{\text{prestress,1}}$ denotes the modal stiffness matrix due to the application of a unitary parametric force.

In the ideal case where $\mathbf{M}^*$, $\mathbf{C}^*$, $\mathbf{K}^*$ and $\mathbf{K}^*_{\text{prestress,1}}$ are diagonal, the N equations of system (3) can be decoupled and the dynamics of the structure in the different mode shapes can be studied separately. In such a case, the system of N coupled equations behaves like N single-degree-of-freedom uncoupled equations. By definition, matrices $\mathbf{M}^*$ and $\mathbf{K}^*$ are diagonal. Matrix $\mathbf{C}^*$ is also diagonal due to the assumption of modal damping. By contrast, there is no reason for matrix $\mathbf{K}^*_{\text{prestress,1}}$ to be perfectly diagonal. Actually, it can be verified that its diagonal elements are only one order of magnitude larger than its out-of-diagonal elements. As long as the product of $F_u(t)$ by the out-of-diagonal elements of $\mathbf{K}^*_{\text{prestress,1}}$ is well below the diagonal elements of $\mathbf{K}^*$, the coupling between modes remains small. In the following, parametric excitations of small amplitudes will be considered in order to limit the excitation of nonlinearities and to keep a quasi-Hamiltonian system. It is therefore expected that this condition will be met to good approximation.

According to these assumptions, the equations of motion can be decoupled for each modal coordinate. The single-degree-of-freedom equation governing the i-th modal coordinate takes the form

$$m_{\text{eq}}\ddot{z}(t) + c_{\text{eq}}\dot{z}(t) + [k_{\text{eq}} + F_u(t)k_{\text{p,eq}}]z(t) = p(t), \tag{4}$$

where $z(t) = q_i(t)$, the equivalent parameters m_{eq}, c_{eq}, k_{eq} and $k_{\text{p,eq}}$ are the generalized parameters of mode i defined according to [2] as the diagonal elements of the modal matrices normalized by $[\mathbf{\Phi}(x_i, i)]^2$, where x_i is the coordinate of an antinode of vibration of mode i, and $p(t)$ is the participation factor of the forced excitation to mode i,

$$p(t) = \frac{\mathbf{\Phi}(x_w, i)}{[\mathbf{\Phi}(x_i, i)]^2} F_w(t) = \alpha F_w(t), \tag{5}$$

where x_w is the coordinate where the forced excitation is applied.

In conclusion, for parametric excitations of sufficiently small amplitude, the modal responses of the structure are uncoupled. If the structure is excited in such a way that it responds only (or mainly) in a unique mode, then the response of the structure at a given point is the solution of an equivalent single-degree-of-freedom equation of the form (4), which is a linear Mathieu equation that can be rewritten in the dimensionless form of Equation (1). Indeed, introducing the characteristic time $T_{\text{charact}} = \sqrt{m_{\text{eq}}/k_{\text{eq}}}$ and the dimensionless time $\tau = t/T_{\text{charact}}$ and defining

$$\xi = \frac{c_{\text{eq}}}{2\sqrt{k_{\text{eq}} m_{\text{eq}}}}, \quad u(\tau) = F_u(\tau)\frac{k_{\text{p,eq}}}{k_{\text{eq}}} \quad \text{and} \quad w(\tau) = \frac{\alpha F_w(\tau)}{k_{\text{eq}}}, \tag{6}$$

Equation (4) becomes

$$z''(\tau) + 2\xi z'(\tau) + [1 + u(\tau)]z(\tau) = w(\tau), \tag{7}$$

where $z'(\tau)$ denotes the first derivative of z with respect to the dimensionless time τ.

4.2 Validity of the single-degree-of-freedom governing equation

Different aspects of the problem have to be taken into account to select the mode used for the reduction. First, the equivalent parameters of the selected mode must allow to cover the largest possible part of the first passage time map in a limited amount of time. Then, to ensure that the other modes have little influence on the dynamics, the selected mode must be such that the out-of-diagonal terms of $\mathbf{K}_{\text{prestress,1}}$ are much smaller than the diagonal elements. The chosen natural frequency must be far enough from other natural frequencies in order to avoid multi-modal excitation of the structure. Based on these remarks, the second bending mode is selected. It is characterized by the equivalent parameters

$$k_{\text{p,eq}} = 39 \text{ m}^{-1}, \quad k_{\text{eq}} = 3\,273 \text{ Nm}^{-1}, \quad c_{\text{eq}} = 0.08 \text{ N[m/s]}^{-1} \quad \text{and} \quad m_{\text{eq}} = 0.05 \text{ kg}. \tag{8}$$

The frequency of this second bending mode is $f_0 = 39.3$ Hz.

In order to identify the conditions under which an efficient use of the reduction of the multi-degree-of-freedom system can be done, both single-degree-of-freedom and multi-degree-of-freedom equations of motion are integrated forward in time using a Newmark integration scheme. On the one hand, the equations of motion of the multi-degree-of-freedom system (2) subjected to given stochastic forced and parametric excitations are solved and the response at an antinode of vibration of the studied mode is extracted. On the other hand, the reduced single-degree-of-freedom equation of motion (4) is solved for the same excitations. The objective is the determination of excitation characteristics that provide a satisfying superposition of the two responses. The modal responses are compared at an antinode of vibration in order to minimize the influence of the other modes.

The forced excitation needs to be defined on a limited frequency band centered on f_0, otherwise, several modes are excited and the single- and multi-degree-of-freedom governing equations provide qualitatively different solutions. When the system is subjected to a forced excitation only, a good match is observed between the responses of the single- and multi-degree of freedom governing equations as long as the frequency band is contained in $[0.8f_0\,;\,1.2f_0]$. When the frequency interval is expanded beyond [$0.8f_0$; $1.2f_0$], the closest modes are excited in such a way that the reduction is not legitimate anymore.

The uncoupling of the equation remains valid as long as the diagonalization of the equations is valid. F_u should therefore remain sufficiently small so that the out-of-diagonal elements of $F_u(t)\mathbf{K}^*_{\text{prestress,1}}$ remain small with respect to the diagonal elements of $\mathbf{K}^*$.

The well known theory of the deterministic Mathieu equation highlights that parametric instabilities occur for parametric excitation frequencies close to $2f_0/k$ (k integer) [1], even if the instability becomes less critical when damping increases. In this stochastic context, the frequency bandwidth of the parametric excitation must be sufficiently small to avoid triggering the other modes of the structure. It is numerically observed that the frequency interval should not include the second harmonics of the other bending modes, unless they are sufficiently damped.

5 Influence of narrow-band excitations on first passage time

The analytical results about first passage time of systems governed by Equation (7) rely on the assumption of broadband white noise excitations. The forced and parametric excitations w and u are characterized by constant power spectral densities S_w and S_u. The Hamiltonian of the quasi-Hamiltonian system (w, u and $\xi \ll 1$) is defined as

$$H = \frac{z^2}{2} + \frac{[z']^2}{2}. \tag{9}$$

The analytical studies conducted in the case of broadband excitations allowed to derive closed-form expressions of the mean first passage time U_1 [9]. They revealed that the reduced average first passage time $U_1 S_u/4$ only depends on the reduced initial energy and energy increment

$$H_0^* = \frac{H_0 S_u}{2S_w} \quad \text{and} \quad \Delta H^* = \frac{\Delta H S_u}{2S_w} \tag{10}$$

and on the damping factor $a = 8\xi/S_u$. This suggests to represent the results by maps of the reduced average first passage time $U_1 S_u/4$ as a function of H_0^* and ΔH^*. For instance, Fig. 7 (dotted lines) represents the analytical results for an undamped system and highlights the three regimes. For $H_0^* \ll 1$, $U_1 S_u/4$ is independent from H_0^*. This is called the additive regime. For $H_0^* \gg 1$, the curves show constant slope and the first passage time depends on by how much the initial energy level is multiplied to obtain the target energy level, which corresponds to the multiplicative regime. The incubation regime in which $U_1 S_u/4$ scales linearly with ΔH^* is identified for $\Delta H^* \ll 1 + H_0^*$.

In the current case, it was shown to be necessary to limit the frequency bands of the excitations for the response of the multi-degree-of-freedom system to be approximated by the response of an equivalent single-degree-of-freedom system. This section is therefore devoted to the numerical study of the influence of such limitations on the frequency band on the first passage time of the single-degree-of-freedom oscillator. The forced and parametric excitations w and u are defined as narrow-band random processes of constant power spectral densities S_w and S_u.

5.1 Influence of the frequency band of the forced excitation

As a first step, the system is studied for broadband parametric excitations and several different narrow frequency bands for the forced excitation (including the natural frequency f_0 of the oscillator or not). The first passage time maps are obtained numerically using Monte Carlo simulations. The Hamiltonian H of the single-degree-of-freedom system is computed at each time step. When it reaches a given maximal value, the simulation is stopped and a new simulation is initiated. The average first passage time is eventually obtained by averaging the results of a large set of simulations.

The three incubation, additive and multiplicative regimes can only be recovered if the frequency band of the forced excitation includes the natural frequency of the system. Fig. 7 compares the analytical map obtained under the assumption of broadband excitations with the numerical map built by Monte Carlo simulations of the oscillator subjected to broadband parametric excitation and narrow-band forced excitation in the interval $[0.8 f_0\,;\, 1.2 f_0]$ ($a = 0$, $S_u = 10^{-3}$, $S_w = 5 \cdot 10^{-4}$). For limited frequency intervals around the natural frequency of the oscillator, a nearly perfect match between the numerical (*i.e.* for narrow-band excitations) and analytical (*i.e.* for broadband excitations) results is observed in the whole map. The results are only significantly different in the bottom left corner corresponding to small values of H_0^* and ΔH^*. This is not surprising since the bottom left corner corresponds to the limit case where there is no parametric excitation; the forced excitation therefore has a dominant influence in this zone.

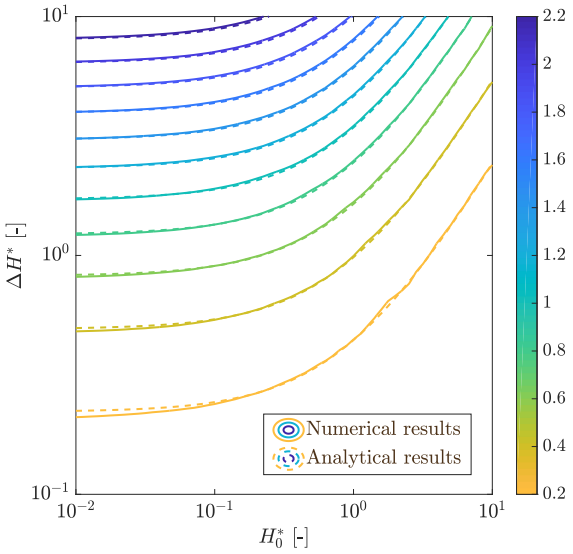

Figure 7: Reduced average first passage time $U_1 S_u/4$. Comparison of the maps obtained numerically for broadband u and narrow-band w on $[0.8f_0\,;\,1.2f_0]$ and analytically for broadband excitations ($a = 0$, $S_u = 10^{-3}$, $S_w = 5 \cdot 10^{-4}$).

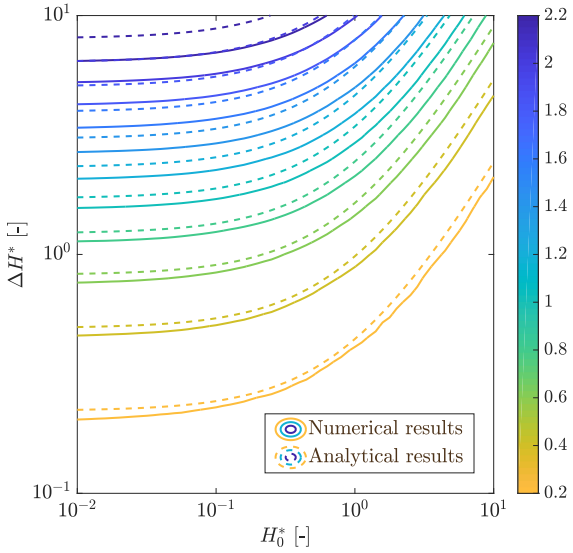

Figure 8: Reduced average first passage time $U_1 S_u/4$. Comparison of the maps obtained numerically for narrow-band excitations (u on $[0.1f_0\,;\,3f_0]$ and w on $[0.8f_0\,;\,1.2f_0]$) and analytically for broadband excitations ($a = 0$, $S_u = 10^{-3}$, $S_w = 5{\cdot}10^{-4}$).

5.2 Influence of the frequency band of the parametric excitation

Fig. 8 compares the maps obtained numerically for narrow-band excitations (F_u on $[0.1f_0\,;\,3f_0]$ and F_w on $[0.8f_0\,;\,1.2f_0]$) and analytically for broadband excitations in the absence of damping ($a = 0$, $S_u = 10^{-3}$, $S_w = 5 \cdot 10^{-4}$). Visual inspection of the maps reveals that the analytical results are not recovered when the system is subjected to narrow-band random processes. Although the additive, multiplicative and incubation regimes can still be clearly identified, the curves do not superimpose. This means that the analytical results obtained for broadband excitations do not simply transfer to narrow-band random processes. Here, the frequency band is limited and the corresponding first passage times are larger than those computed with broadband excitations. A more systematic study is required to characterize the influence of the parametric excitation.

The undamped system ($a = 0$) is studied. The parametric excitation is defined as a narrow-band process of constant power spectral density $S_u = 10^{-3}$ on the frequency interval $[f_1\,;\,f_2]$ and the bounds f_1 and f_2 are varied. The forced excitation is defined as a narrow-band process of constant power spectral density $S_w = 5 \cdot 10^{-4}$ on the frequency interval $[0.8f_0\,;\,1.2f_0]$, in agreement with the conclusions of the previous section.

An indicator I is introduced and defined as

$$I = \left| \frac{U_1^{\mathrm{MC}} - U_1^{\mathrm{th}}}{U_1^{\mathrm{th}}} \right|, \tag{11}$$

where U_1^{MC} and U_1^{th} are respectively the mean first passage time obtained from Monte Carlo simulations with narrow-band processes at some observation point of the map and the corresponding analytical mean first passage time for broadband processes. Based on the comments of the previous section, the initial energy H_0^* and the energy increment ΔH^* are chosen far from the bottom left corner of the map where the influence of the narrow band of the forced excitation is large and for moderate values of H_0^* and ΔH^* to limit the computation time.

Fig. 9 shows the value of the indicator I (11) as a function of the lower and upper frequencies f_1 and f_2 (normalized by the natural frequency f_0) that define the parametric excitation at the observation point of the map characterized by $H_0^* = 10^{-1.5}$ and $\Delta H^* = 10^0$. This figure shows that it is necessary to include the second harmonic of the natural frequency, $2f_0$, in the frequency interval to be close enough to the analytical results for broadband excitations. In fact, when the second harmonic of the natural frequency does not belong to the frequency interval of the parametric excitation, the first passage time map looks completely different; even the three regimes do not appear. By contrast, it is not necessary to include the natural frequency itself in the frequency interval $[f_1\,;\,f_2]$. This can be supported by the deterministic theory of Mathieu equation [1]. Instabilities occur at frequency $2f_0/k$ (k integer). While the instability for $k = 1$, *i.e.* at $f = 2f_0$, is the most critical, the other instabilities do not develop when forced excitation or damping is introduced in the system unless the amplitude of the parametric excitation is large.

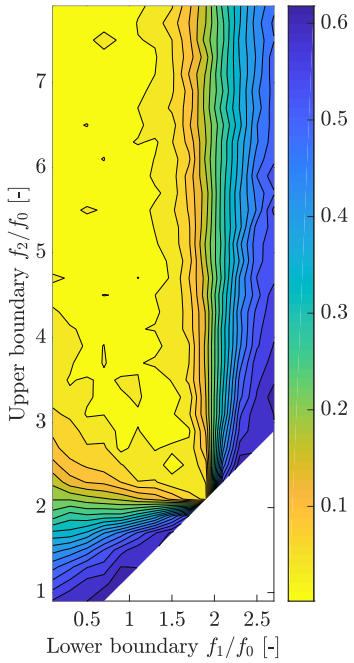

Figure 9: Indicator I (11) at point $H_0^* = 10^{-1.5}$ and $\Delta H^* = 10^0$ as a function of the lower and upper frequency of the bandwidth of the parametric excitation ($a = 0$, $S_u = 10^{-3}$, $S_w = 5 \cdot 10^{-4}$).

It should be noted that, even if this study is based on a single point of the map located in the additive regime, the same exercise has been performed at other points located in other regimes and the same general conclusions have been drawn. The numerical study of systems characterized by other values of a, S_w and S_u also lead to the same general conclusions.

6 Experimental study of first passage time

The above numerical studies provide useful information to prepare the experimental study of first passage time. The forced excitation F_w and the parametric excitation F_u applied to the experimental set-up (Fig. 1) must be such that the conditions for the model reduction to be valid are verified and the influence of the narrow bands remains limited.

The forced excitation F_w is defined as a narrow-band process of constant power spectral density $\tilde{S}_w = 5 \cdot 10^{-3}$ N^2/Hz on the frequency interval $[0.87f_0\,;\,1.13f_0] = [34\,;\,44]$ Hz. This frequency interval does not cover any of the other natural frequencies of the set-up. The parametric excitation F_u is defined as a

narrow-band process of constant power spectral density $\tilde{S}_u = 5 \cdot 10^{-3}$ N^2/Hz on the frequency interval $[0.77 f_0\,;\, 2.57 f_0] = [30\,;\, 100]$ Hz. This frequency interval covers the natural frequency f_0 and its second harmonic. It can be regretted that the second harmonic of the first bending mode and the natural frequency of the third bending mode are also included. But, this is not an issue thanks to the high damping ratios of these modes.

Equation (6) shows that the dimensionless parameters a, S_w and S_u are related to the dimensional parameters through

$$a = \frac{4 c_{\text{eq}} k_{\text{eq}}}{k_{\text{p,eq}}^2 \tilde{S}_u} = 132,\ S_w = \frac{\tilde{S}_w}{T_{\text{charact}}} \left(\frac{\alpha}{k_{\text{eq}}} \right)^2 = 2.5 \cdot 10^{-10} \text{ and } S_u = \frac{\tilde{S}_u}{T_{\text{charact}}} \left(\frac{k_{\text{p,eq}}}{k_{\text{eq}}} \right)^2 = 1.8 \cdot 10^{-4}. \quad (12)$$

The force intensities S_w and S_u are much smaller than one, as required by the theory to have a quasi-Hamiltonian system. The high value of a does not mean that damping is intrinsically high ($\xi = 4 \cdot 10^{-3} \ll 1$) but, merely, that damping is high with respect to the amplitude of the parametric excitation.

The structure is excited by the horizontal and vertical shakers for 30 minutes and the velocity of the structure is measured at a vibration antinode with the laser transducer. The response is numerically integrated to compute the evolution of the position with time. It is then checked that the structure responds only in its second bending mode by analyzing the response in the frequency domain. The dimensionless Hamiltonian corresponding to Equation (7) is eventually computed by Equation (9).

The average first passage time map corresponding to the evolution of the Hamiltonian of the system with time can be built from the experimental results (solid lines in Fig. 10). If the time signal is sufficiently long, the same level of energy is reached several times and the system passes many times from initial energies H_0 to higher energies $H_c = H_0 + \Delta H$. Both energy axes are discretized in a finite number of values. The intervals between these values are chosen with uniform sizes on a logarithmic scale as this is the physical scaling suggested by the stochastic model. The mean first passage time corresponding to each point of the map (*i.e.* each combination of initial energy H_0^* and energy increment ΔH^*) is obtained by averaging all the first passage times corresponding to the transitions between these levels of energy [8].

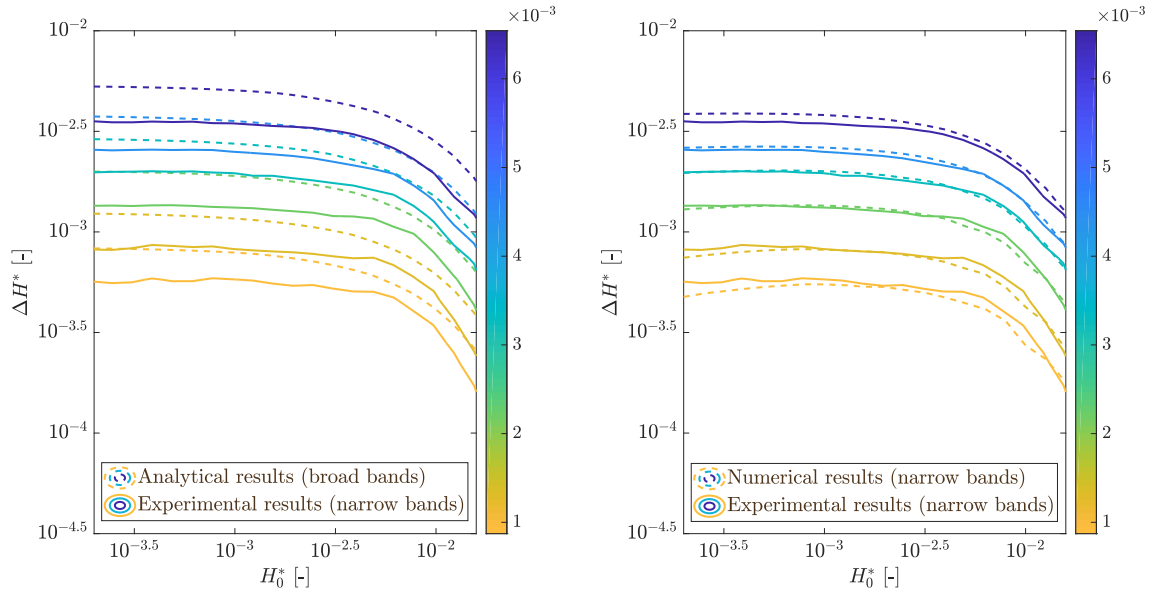

(a) (b)

Figure 10: Reduced average first passage time $U_1 S_u / 4$ as a function of H_0^* and ΔH^*. Comparison of the maps obtained experimentally and numerically for narrow-band excitations (F_u on $[0.77 f_0\,;\, 2.57 f_0]$ and F_w on $[0.87 f_0\,;\, 1.13 f_0]$) and analytically for broadband excitations ($a = 132$, $S_w = 2.5 \cdot 10^{-10}$, $S_u = 1.8 \cdot 10^{-4}$).

Fig. 10(a) compares the experimental results with the analytical map obtained under the assumption of broad-band excitations. The results are qualitatively similar and the general trend of the average first passage time is recovered experimentally but, as expected, the curves do not superimpose.

Fig. 10(b) compares the experimental results with the map obtained by Monte Carlo simulations of the numerical system subjected to the same narrow-band excitations as in the experimental tests. Globally, a good match between the maps is observed and the global behavior of the mean first passage time is recovered. The different regimes can be analyzed separately.

The additive regime is well represented. In the left part of Fig. 10(b), the experimental curves tend towards horizontal asymptotes, at least for sufficiently large values of the increment ΔH^*. The incubation regime can be highlighted by considering cross-sections of the map at constant values of H_0^*. Fig. 11 shows the evolution of the average first passage time as a function of ΔH^* for $H_0^* = 2 \cdot 10^{-2}$ and $2 \cdot 10^{-3}$. As hinted by the linear trends represented as a guide, the average first passage times (cross markers) are fairly well aligned, which is the specific feature of the incubation regime.

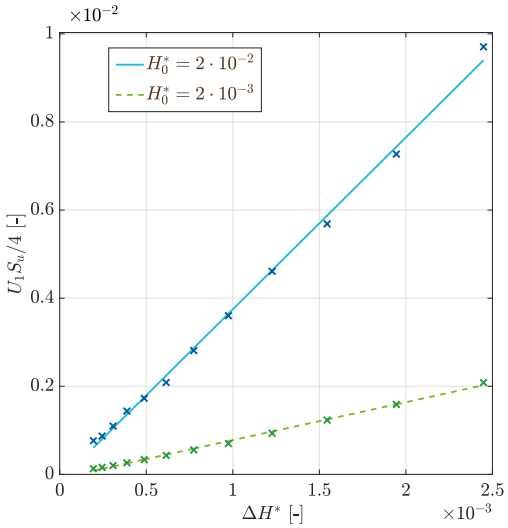

Figure 11: Cross-sections of the reduced average first passage time map (Fig. 10) in the incubation regime for $H_0^* = 2 \cdot 10^{-2}$ and $H_0^* = 2 \cdot 10^{-3}$. Experimental data (crosses) and linear trend (lines).

The multiplicative regime cannot be rigorously observed in Fig. 10(b). In the right part of the figure, the curves show the same negative slope but the multiplicative regime is not yet reached since the highest value of H_0^* is of the order of $10^{-1.5}$ while the multiplicative regime appears for $H_0^* \gg 1$. On the one hand, such high values of H_0^* must be avoided here since it can cause the excitation of nonlinearities in the system. On the other hand, for damped systems subjected to broadband excitations, the asymptotic slope in the multiplicative regime equals $2 - a$. This result is certainly not directly valid in the narrow-band excitations case but suggests that, given the high value of $a = 132$, the part of the multiplicative region reachable in a limited amount of time reduces to the bottom right corner. Because this corner is characterized by high coefficients of variation [10], very long time signals would be required to get a smooth map in this region.

The differences between the numerical and experimental results can be ascribed to different factors. The experimental conditions never match exactly the numerical ones. For instance, the power spectral densities of the excitations are not perfectly constant on the frequency band of definition, and do not drop to zero outside this interval. Then, the structure is inherently a multi-degree-of-freedom system and it is not possible to excite a single mode of the structure. Structure nonlinearities can also be a source of differences between the numerical and experimental results. Indeed, even if the intensities of the excitations have been chosen extremely small to limit the excitation of the nonlinearities, those are inherent to the structure.

7 Conclusions and perspectives

This work aims at designing and testing an experimental set-up to illustrate and provide empirical evidence of the main analytical results of the theory of first passage time described in [9]. The current theory applies to quasi-Hamiltonian linear single-degree-of-freedom systems subjected to broadband forced and parametric excitations (δ-correlated Brownian processes).

The selected structure consists in a vertical steel strip pre-stressed by a mass. First, a finite element model of the structure is built. The inherently multi-degree-of-freedom system is reduced to match the assumption of a single-degree-of-freedom system behind the theory of first passage time. This is done by defining the forced and parametric excitations as narrow-band random processes triggering only one bending mode of the structure. Since analytical results are not available for the first passage time of systems subjected to narrow-band excitations, a numerical study is performed and some general conclusions are drawn about the influence of the frequency bands of the forced and parametric excitations on the first passage time. The global behavior of the average first passage time is recovered in the whole map as long as the natural frequency of the oscillator is included in the frequency band of the forced excitation and the frequency band of the parametric excitation contains the second harmonic of the natural frequency. When these conditions are met, small quantitative differences can be observed when broadband or narrow-band excitations are used but the dynamics remains qualitatively similar.

The previous steps provide a rationale for selecting the appropriate parameters of the experimental testing. The experimental first passage time map is built and compared with the theoretical and model results. A good quantitative match is observed between the experimental map and the numerical results obtained with Monte Carlo simulations with narrow-band excitations. The experimental results are also qualitatively similar to the theoretical ones for broadband excitations. Both the additive and incubation regimes are clearly identified. Only the beginning of the multiplicative regime can however be observed.

This study contributes to broadening the scope of the first passage time theory introduced in [9, 10] beyond the context of single-degree-of-freedom linear systems subjected to broadband excitations considered so far by numerical and experimental studies of oscillators subjected to narrow-band processes. It is also a first physical evidence that the first passage time of real multi-degree-of-freedom mechanical systems can be characterized with the physical properties of the structure.

This study also suggests that work is still needed to go further with analytical, numerical and experimental studies of systems subjected to narrow-band excitations. In particular, analytical studies of the first passage time of systems subjected to colored excitations, and in particular to narrow-band excitations, could be conducted to get a better insight into the phenomena.

References

[1] M. Cartmell, *Introduction to Linear, Parametric and Nonlinear Vibrations*, Springer, 1st ed. (1990).

[2] D. Ewins, *Modal Testing: Theory, Practice and Application*, Research Studies Press Ltd, 2nd ed. (2000).

[3] M. Géradin, D. J. Rixen, *Mechanical Vibrations: Theory and Application to Structural Dynamics*, Wiley, 3rd ed. (2015).

[4] M. Gitterman, *Spring pendulum: Parametric excitation vs an external force*, Physica A: Statistical Mechanics and its Applications, Vol. 389 (2010), pp. 3101-3108.

[5] J. L. Lilien, A. Pinto da Costa, *Vibration Amplitudes Caused by Parametric Excitation of Cable Stayed Structures*, Journal of Sound and Vibration, Vol. 174 (1994), pp. 69-90.

[6] A. A. Prikhodko, A. V. Nesterov, S. V. Nesterov, *Analysis of Mathieu Equation Stable Solutions in the First Zone of Stability*, Procedia Engineering, Vol. 150 (2016), pp. 341-346.

[7] P. van Overschee, B. L. de Moor, *Subspace Identification for Linear Systems: Theory - Implementation - Applications*, Springer US, 1st ed. (1996).

[8] H. Vanvinckenroye, T. Andrianne, V. Denoël, *First passage time as an analysis tool in experimental wind engineering*, Journal of Wind Engineering and Industrial Aerodynamics, Vol. 177 (2018), pp. 366-375.

[9] H. Vanvinckenroye, V. Denoël, *Average first-passage time of a quasi-Hamiltonian Mathieu oscillator with parametric and forcing excitations*, Journal of Sound and Vibration, Vol. 406 (2017), pp. 328-345.

[10] H. Vanvinckenroye, V. Denoël, *Second-order moment of the first passage time of a quasi-Hamiltonian oscillator with stochastic parametric and forcing excitations*, Journal of Sound and Vibration, Vol. 427 (2018), pp. 178-187.

[11] Siemens website. `http://www.plm.automation.siemens.com`. Last view 24th May 2018.